IJASRM
International Journal of Advanced Scientific Research and Management, Vol. 2 Issue 11, Nov. 2017.
www.ijasrm.com
ISSN 2455-6378

Effect of Ni doping on Structural and optical properties of $Ni_xCd_{1-x}S$ nanoparticle synthesized by chemical precipitation method

Anil Kumar[1*], Ramesh K. Sharma[1], Navdeep Goyal[2], Sanjeev Gautam[3]

[1]University Centre for Instrumentation & Microelectronics (UCIM), Panjab University, Chandigarh - 160 014, India,
[2].Department of Physics, Panjab University, Chandigarh - 160 014, India

[3].Dr. S.S. Bhatnagar University Institute of Chemical Engineering & Technology, Panjab University, Chandigarh - 160 014, India

Abstract

Effect of nickel doping was investigated on Cadmium Sulphide nanoparticles (CdS NP) synthesized by chemical precipitation technique. The synthesized nanoparticles were systematically characterized with XRD, FE-SEM/TEM, UV-vis and FTIR spectroscopy. XRD analysis confirmed the Zinc-blende nanostructure for all samples. The crystallite size for 0.5M CdS NP showed a decrease from 5.27 nm to 3.40 nm on doping, whereas the strain(%) parameter increased from 0.35 to 4.33. Similar trend was observed in case of 1.0M CdS NP too. SEM micrographs indicated grain size approximately 20 nm for all samples. The Band Gap showed a blue shift from 2.40 eV to 2.58 eV for 0.5M on doping and for 1.0M it was from 2.45 eV to 2.53 eV, as shown by UV-vis measurements. The shift in FTIR (642 cm^{-1}) revealed the incorporation of Ni-atom at Cd-site in CdS host matrix lattice. The band gap blue-shift makes the material useful for the optoelectronics device applications.

Keywords: CdS, Nanoparticle, optical properties, Light sensor, Characterization, doping.

1. Introduction

For nanocrystalline semiconductors, size-dependence of the band gap(Eg) is most important consequence of the quantum confinement effect. Band gap may be tuned to a precise energy depending on the degree and dimensionality of confinement. The continuous tuning of band gap in II-VI semiconductors is due to unique positive deformation potential. For applications of photo- voltaic devices, it is important to engineer nano crystals for efficient charge carrier separation & multi exciton generation[1]. For ultra-nanoparticle when nano crystallite radius < 2 exciton Bohr radius(α_B = 3nm) confinement becomes larger than columbic interaction and hence electron and holes are considered as two confined particles which are bound by an enforced coulomb interaction [2–5]. Quantum confinement in low dimensional structures enables band-gap engineering (by varying nanoparticle radius and high quality surfaces) and makes them suitable for tera-Hz applications [6]. Effects of strain in semiconductor nanocrystals in both the colloidal and solid state phase have a great impact. The dislocations arise from strain, modifies the bond length and hence alters the electronic band gap, as the valence and conduction band edge energy is derived from the bond strength. Activation energy (Eg) of nanocrystals (e.g. for CdS Eg = 2.42 eV) may be tuned to emit fluorescent light in the visible spectrum that will be useful for optoelectronic devices[1, 7].

The band gap is the most important parameter of semiconductors which affects their optical, electrical and electronic properties. For an electron to jump from Valance Band (VB) to Conduction Band (CB), it needs energy hv equal to its electronic band gap, leaving behind a vacancy (hole). If a photon has more energy than the band gap, then its absorption will excite electron from lower VB to higher CB. However, the excess energy is lost through inelastic collisions as the electron settles to the bottom of the CB and the hole rises to the top of the VB. The electron always returns to its ground state through electron-hole recombination process in which a photon is emitted having energy equal to the band gap. For decreasing size of a semiconductor crystal, starting from bulk to quantum dot (QD) the allowed

energy levels gradually broaden and become more discrete. In nano-structured semiconductors, the edges of the band structure are not completely developed and show more discrete levels with Fermi energy lying in the band gap. For QD or nanoclusters the orbitals are developed into CB and VB. The highest occupied molecular orbital (HOMO) becomes the top of the VB and the lowest unoccupied molecular orbital (LUMO) becomes the bottom of the CB[8, 9]. The decreasing size of semiconductor crystal leads to the broadening of band gap. The electrons, holes and excitons in nano crystallites have limited space to move and their motion is possible only for definite values of the energy. Consequence of this, the continuum of states in the CB and VB are broken down into discrete states with energy spacing approximated by inverse of the square of crystallite radius. Hence, broadening of the band gap in comparison to the bulk takes place, i.e., a blue shift in the optical absorption spectra[10].

For the last several years, nanostructured materials have been the subject of intense study due to their size dependence physical and chemical properties. Nanoparticles have a large proportionate number of surface atoms compared to the bulk, therefore characteristic of surface atoms have relatively more contribution towards their properties. Cadmium sulphide is one of the most important group (II-VI) elements having size tunable optical and electrical properties [11, 12]. The transition metal dopants in host semiconductor (group II-VI) introduce disorder and spin-orbit interactions may induce magnetic ordering that leads to dilute magnetic semiconductor (DMS) [13–15]. Semiconductors doped with transition metal element or rare earths have attracted much attention due to their applications in spintronics [16–18]. Effect of dopant with CdS has been discussed. The Eg of CdS has been found to decrease due to diffusion of Ni-ion into host lattice[19, 20]. In the present study, the CdS nanoparticles were synthesized using chemical reaction precipitation method. Further Ni doped CdS nanoparticles were systematically investigated and results are accounted for and interpreted.

2. Materials and Methods

In co-precipitation technique used in this work, cadmium acetate, nickel acetate and sodium sulphide (99.99%, Sigma Aldrich) were used as purchased. For preparing undoped 0.5M concentration solutions, 13.32 g of cadmium acetate and 6.60 g of sodium sulphide were dissolved in two separate beakers containing 100 ml of double distilled water each. Sodium sulphide solution was mixed drop wise in this cadmium acetate solution being stirred constantly at room temperature (300K), as discussed in equations [(1) & (2)]. The whole solution was centrifuged at 8000 rpm for 10 minutes and washed about six times with distilled water and methanol respectively. This product was dried at 80^{o}C in oven for about 24 hours and allowed to cool down to room temperature. It was ground into a fine powder for further characterization. For Ni-doped (5 at.%) 0.5 M solution, three beakers of cadmium acetate(13.32 g), Sodium sulphide(6.60g) and Nickel acetate (24.84 g) were prepared in 100 ml double distilled water each. Now, 5 ml of cadmium acetate was taken out and discarded, and then in the same beaker of cadmium acetate, 5 ml of nickel acetate (from 100 ml of nickel acetate beaker) was added (for Ni-doping). This beaker was kept on ultrasonic cleaner for about 10 minutes to mix it properly. Now, sodium acetate was added drop wise to the cadmium acetate mixed with nickel acetate solution and solution was constantly stirred at room temperature. After completing this process, the solution was left undisturbed, so that precipitates settle down completely. This solution was then washed with distilled water and methanol respectively by ultrasonic mixing/cleaning and then centrifuging. The process is repeated about 8 times, to ensure that soluble impurities were not present in the final sample. This sample was dried at 80^{o}C for 24 hours and allowed to cool down to room temperature. Finally dried powder of Ni-doped CdS was obtained and ground for further characterization.

$$Cd(CH_3COO)_2 + Na_2S \rightarrow CdS + 2Na(CH_3COO) \quad \ldots(1)$$

$$\{Cd(CH_3COO)_2 + Ni(CH_3COO)_2\} + Na_2S \rightarrow Ni_xCd_{1-x}S + 2Na(CH_3COO) \quad \ldots(2)$$

Similarly for preparing 1.0 M concentration solution, 26.65g of cadmium acetate, 13.21g of sodium sulphide and 24.84g of nickel acetate were taken and repeated the whole process.

The structure of pure and Ni(5%) doped CdS nanoparticles were analyzed by X-ray diffraction (XRD) pattern performed at PANalytical X-ray diffractometer using CuKα radiation (λ = 1.54012^{o}A) in the range of 20^{o}- 60^{o} (2θ) at scanning rate of 0.05^{o}/min. UV-vis absorption spectra were collected using UV-vis spectrophotometer(Lambda 750 PerkinElmer) and FTIR spectra were taken by PerkinElmer(400 FTIR) Spectrometer. Transmission Electron Microscopy (TEM) micrographs were obtained by Hitachi (H-7500) and the surface morphology was examined by FE-SEM Hitachi (SU 8010)

IJASRM
International Journal of Advanced Scientific Research and Management, Vol. 2 Issue 11, Nov. 2017.
www.ijasrm.com
ISSN 2455-6378

3. Results and Discussion

3.1 Structural study

XRD technique gives relevant information about crystallinity, structure and strain of materials. Fig 1(a,b) showed the XRD pattern for doped and undoped CdS NP at different molar concentrations. The characteristic peaks (111), (220) and (311) corresponding to diffraction 2θ = 26.49°, 43.61° and 52.23° showed good crystalline nature of prepared samples and well matched with cubic zinc-blende phase of CdS (JCPDS 10-454) as shown in Fig. 1(a & b). To override the possibility of presence of hexagonal structure, the characteristic peaks were deconvoluted as shown in the insets of Fig.1(a & b), which shows the absence of any extra peak related to hexagonal structure and other crystal structure than zinc-blende phase. Hence, the crystal-size was calculated within the limits of XRD technique. The crystallite size may be approximated due to ultra-nano synthesized particles, which leads to the development of exciton confinement [2, 3]. Broadening of peaks in the diffraction pattern is characteristic feature of nanomaterials due to random orientation of crystals. Also, inhomogeneous lattice strain and structural disorder are responsible of broadening of peaks in the diffraction pattern[21]. Peak broadening estimates the crystallite size, which further calculates factors like, lattice strain and structural disorder. The crystallite size was calculated using Debye-Scherer[22] equation

$$D = K\lambda/\beta \cos\theta$$

where D is crystallite size, λ is diffraction wavelength used and β is corrected FWHM(full width half maxima), K is the constant and is close to unity and θ is diffraction angle. The value of β can be obtained from observed FWHM by convoluting Gaussian profile. The crystalline size as calculated was found to vary from ~ 5.27 nm to ~3.75 nm with Ni-doping for 0.5M, while it changed from ~3.40 nm to ~2.40nm for 1.0M concentration. The calculated crystallite size along with strains shown in Table 1 for undoped and doped CdS in both concentrations. It is clear from the Table 1, that size decreases on Ni-doping at both concentrations, while strain increases. The diffraction pattern for (111), (220) & (311) peak position shows a clear shift (~0.02°) towards higher angle (i.e. corresponds to lower d-values) with increasing Ni-concentration.

This clearly implies lattice compression, consistent with smaller ionic radii of Ni^{+2} (0.69 ˚A) than that of Cd^{+2}(0.97°A) confirming dopant incorporation in the synthesized CdS material. Also substitution of Cd^{+2} by Ni^{+2} decreases the XRD peak intensities of Ni^{+2}

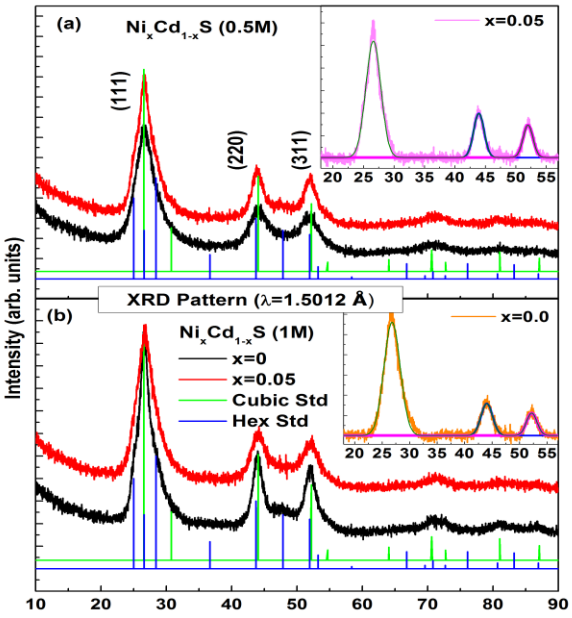

Figure1: XRD pattern for CdS and Ni-CdS nanoparticles synthesized with (a) 0.5M molar conc. and (b) 1.0M molar conc., showing Zinc-blende Cubic structure.

Upon doping, no additional reflection were observed indicating that the cubic phase of CdS structure is not disturbed by nickel substitution. Line Broadening was analyzed by deconvolating size and strain using simplified integral breadth method developed by Williamson & Hall [24]. For deconvolating size and strain contribution to line broadening, a simplified integral breadth method was used. In this method y-intercept can be used to calculate crystallite size and strain can be found from slope. The method of Warren & Averbach [25] taken into account not only the peak width but also the shape of the peak. For obtaining true diffraction profile, this method is based on a Fourier deconvolation of measured peaks and the instrument broadening. So with this method we can calculate both lattice micro strain and crystallite size[26, 27].

Table 1 Table shows the size and strain for undoped and Ni-doped CdS NP

Sr. No	Conc.	FWHM (Degree)	Size (nm)	Strain%
Undoped CdS				
1	0.5M	1.91	5.27	0.35
2	1.0M	2.36	3.40	4.33
Ni (5%) doped CdS				
1	0.5M	2.01	3.75	0.37
2	1.0M	3.43	2.40	6.36

3.1.1 Micro-strain measurements using XRD

The micro-strains are expressed by broadening of the peaks corresponding to the planes which are perpendicular to the micro-strain direction, as

discussed by Warren and Averbach [25]. They identified that broadening is due to size & strain component. The former depends on the size of coherent domains, which is not limited to the grains but may include effects of stacking and subgrain structures. The latter is caused by any lattice imperfections such as dislocations, different point defects or micro-strains. In addition to these two broadening sources, there is also broadening due to the instrumental setup, such as axial divergence, wavelength dispersion, sample transparency, flat sample effect and the detector resolution.

There are many different methods (models) for analysis of these components, which have been divided into two groups: model-dependent and model- independent. The most common model-dependent techniques are the Integral Breadth (IB) [28] method and its simplistic version, the Williamson & Hall(WH) [24] method. The most common model-independent techniques are the Warren-Averbach (WA or the Fourier method)[25] and the Rietveld methods [29]. The WH method is the simplest and most used method but has some contradiction. This method assumes that the contribution of both the strain and the crystallite size to the profile shape are Gaussian-like. It is widely agreed that the profile shape of the strain contribution is Gaussian-like and the size contribution is Lorentzian like. The IB method takes this fact into account.

The basis of the Rietveld technique is to propose a model for the diffraction pattern. It involves the crystalline structure, the experimental array and the background, and contains parameters that characterize each of these parts. Such parameters can be refined by using a least square minimization. The refined parameters are given as lattice parameters, atom positions, the temperature factors associated with the atom vibrations, average micro-strain, grain size, phase concentrations and atom occupancy. This method is widely used, especially for powder analysis, which provide a great deal of information about phase content, particle size, strains etc. The more accurate method was developed by Warren and Averbach[25]. This method assumes that the whole peak profile is described by a Fourier series. The peak shape of a standard material which shows no broadening is also determined and then used to de-convolute the instrumental and sample broadening effects. Because the entire peak profile is used, this approach has both advantages and disadvantages when compared to the WH and IB techniques. Each of the methods mentioned above have their advantages and drawbacks. The Fourier method gives a distribution of crystallite sizes instead of an average value and the correction for instrumental broadening is more rigorous when the shape of peak is not purely Gaussian or Lorentzian. On the other hand, this method is prone to error if peak tails are not accurately modeled. This makes the Fourier methods difficult to use when peak overlap is significant. Furthermore, Fourier decomposition is not always numerically stable. The expression for microstrain(ε) that exist in nanocrystalline material is given by Wilson method as given below

$$\varepsilon = \beta / 4 \tan \theta$$

where β is FWHM and θ is diffraction angle.
Tables 1 depict comparison of crystallite size and strain for undoped and Ni- doped CdS for both concentrations. It is clear that with both kind of concentration and doping, there was a decrease in crystallite size and an increase in strain level. It was also noticed from the Table 2 that gap in the size variation for 0.5 M is higher than the gap for 1.0 M, which shows a trend in the saturation in the doped material.

Table 2 Comparison of band gap (eV) for 0.5M & 1.0M CdS NP

Sr. No	Undoped/doped	FWHM (Degree)	Size (nm)	Band Gap (eV)
0.5M CdS				
1	Undoped	1.91	5.27	2.40
2	Doped (5% Ni)	2.01	3.75	2.58
1.0 M CdS				
1	Undoped	2.36	3.40	2.45
2	Doped (5% Ni)	3.43	2.40	2.52

3.2 Optical analysis

In order to calculate band gap of CdS NP, absorption UV-vis Spectrum were recorded as shown in Fig. 2(a&b). In optical analysis with UV-vis spectrophotometer, 2 mg of synthesized material (0.5M/1.0M un-doped /doped CdS material) was dissolved with methanol. Then mixed ultrasonically for about 20 minutes for uniform distribution and without any delay, sample was loaded for UV-vis measurements. The CdS semiconductor material exhibited less optical absorption for photons with energy, lower and higher than band gap energy. As a result, there is a sharp increase in absorption at energy near to BG that manifest a hump in the absorption spectrum that represent particular characteristic value of CdS material. (So absorption is not increasing with decreasing wavelength below 500 nm) The estimated BG value for un-doped 0.5M CdS NP is 2.4 eV corresponding to absorption edge at 516 nm which is blue-shifted compared with absorption edge of bulk CdS (520 nm). The relation between bandgap and cutoff wavelength is as below

$$E_g = 1240/\lambda_c$$

where λ_c is cutoff wavelength. Band gap for 0.5M

IJASRM
International Journal of Advanced Scientific Research and Management, Vol. 2 Issue 11, Nov. 2017.
www.ijasrm.com
ISSN 2455-6378

and 1.0M, as well as their doping with Ni 5% were taken to see the effective variation. Band gap increases with doping(5% Ni) for 0.5M CdS (Fig. 2(a)) and 1.0M CdS with 5% Ni(Fig. 2(b)). Again it was observed that the difference in band gap with higher concentration is less as compared to lower concentration (0.5M), which indicated that effect of doping is heading towards saturation of host crystal. As also discussed in last section (3.1.1), the gap in the size and strain was lesser for 1.0 M as compared to the 0.5 M concentration.

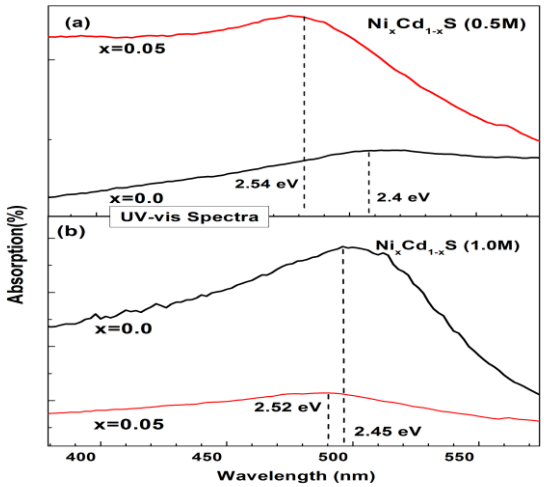

Figure 2 UV-vis spectrum for CdS and Ni-CdS nanoparticles

3.3 FTIR Analysis

In order to support the incorporation of Ni at Cd site in the CdS matrix, FTIR spectra for undoped and Ni-doped CdS for both concentration is shown in Fig. 3. An absorption peak at 653 cm^{-1} associated with CdS stretching has been observed and the shift of CdS stretch toward higher wavenumber (blue shift) and decrease in intensity w.r.t. undoped 0.5M CdS indicates incorporation of Ni^{+2} ions in the CdS host structure. Ni-S stretching band was not observed due to homogeneous substitution of Ni-ion in CdS structure [30]. The lattice of host CdS semiconductor may be perturbed on addition of Ni^{+2} ions and these perturbation should create a frequency shift. For higher molar concentration (1.0M), no-shift was seen with Ni-doping(5%), which may be due saturation of lattice sites. As discussed the FTIR and XRD analysis, no extra peak was observed other than the basic structure of CdS, which indicate that Ni was substituted in place of Cd in the CdS matrix.

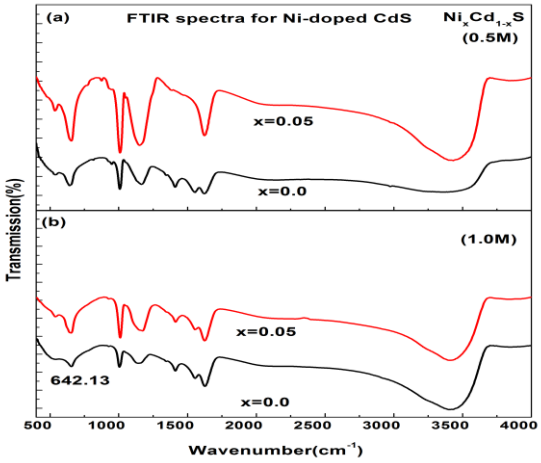

Figure 3 FTIR Spectra for 0.5M CdS undoped and Ni-CdS(1 M) nanoparticles

3.4 Morphology study

3.4.1 FESEM Analysis

Surface morphology of CdS nanoparticle were investigated with FE-SEM as shown in Fig. 4 and 5. It was observed that particles are uniform; and their size and distribution are dependent upon the doping and concentration. The agglomerated average particle size (grain size) was found to be approximately 20 nm. Due to spherical symmetry nano-grains are uniformly distributed in the background throughout the surface and are closely packed. The reason of spherical symmetry might be due to immense surface energy of nano-grains. The cause of grain-clusters may be due to agglomerated atoms and exhibits similar surface morphology with large number of nano-grains of different sizes and also due to reaction between ionic species of free Cd^{+2} ions and free S^{-2} ions.

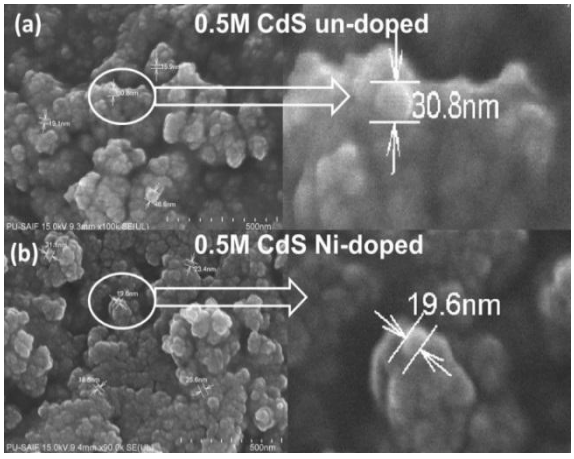

Figure 4 FESEM micrographs for 0.5M CdS undoped and Ni-CdS nanoparticles.

IJASRM
International Journal of Advanced Scientific Research and Management, Vol. 2 Issue 11, Nov. 2017.
www.ijasrm.com
ISSN 2455-6378

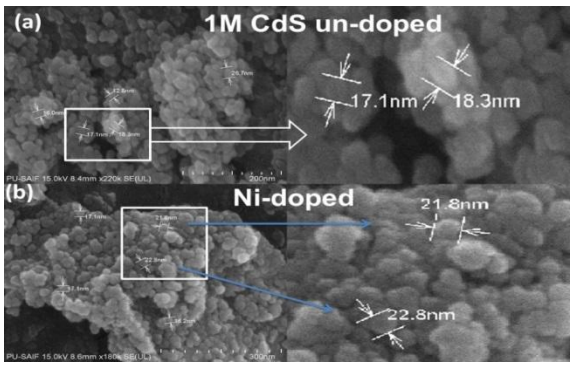

Figure 5 FESEM micrographs for 1M CdS doped Ni-CdS nanoparticles

3.4.2 TEM analysis

TEM micrographs showed the spherical crystallites, which are mono-dispersed and average particle size was in the range of 1.5 nm to 4 nm, which is also been supported by XRD results. Figure 7 correspond to un-doped & doped CdS nanoparticles for 0.5M and 1.0M concentrations. The images indicate that nanoparticles were well defined, visible and no aggregation were formed. The TEM micrograph shows small amount of individually available nano-crystallites and large amount of small nano-crystallites and these are dispersed throughout in the background. In addition to this, TEM micrographs shows a cluster of agglomerated nano-crystallites, adhering to one another indicating the pattern of particles embedded in each other. The TEM micrographs show irregular agglomeration due to variation in the strain value (Table 1), among different size of nanoparticle in corresponding grains.

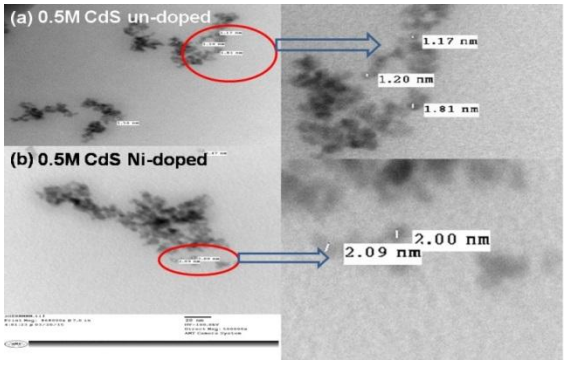

Figure 6 TEM micrographs for 0.5M CdS undoped and Ni-CdS nanoparticles

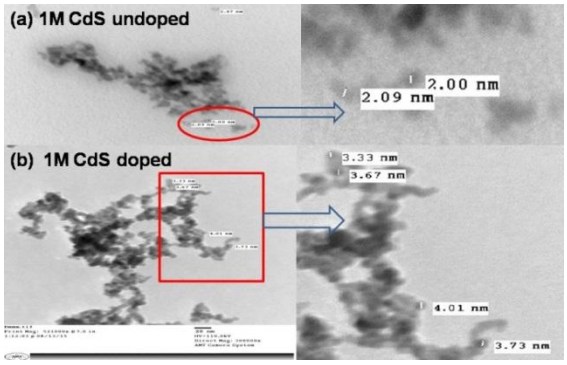

Figure 7 TEM micrographs for 1.0 M CdS undoped and Ni-CdS nanoparticles.

4. Conclusions

Pure and Ni-doped cadmium sulphide nanoparticles were successfully synthesized at room temperature. The XRD pattern showed that undoped and Ni-doped CdS NP have Zinc blende structure with (111), (220) and (311) planes. The crystallite size calculated by XRD measurements was approximately 3 to 5 nm, while TEM gave particles size about 1.5 to 4 nm. UV-vis spectra for undoped and Ni-doped CdS NP showed blue shift in comparison to bulk CdS counterpart, for both concentrations. It was observed that the difference in band gap with higher concentration was less which indicates that effect of doping heading towards saturation of host crystal. FTIR analysis endorsed similar behavior. It is concluded that band gap of CdS show blue shift as material approaches nano size. Further band gap can be tuned with the variation of doping concentration of Nickel. Hence nanoparticles synthesized with such semiconductor may be used for fabricating the devices utilizing these tuning properties.

Acknowledgements: Authors are thankful to Director, Sophisticated Analytical Instrumentation Facility (SAIF), Panjab University Chandigarh for encouragement and support.

References

1. T.L. Chu, S.S. Chu, Solid State Electron. **38**(3), 533 (1995)
2. R. Koole, E. Groeneveld, D. Vanmaekelbergh, A. Meijerink, C. de Mello Doneg´a, *Size Effects on Semiconductor Nanoparticles* (Springer Berlin Heidelberg, Berlin, Heidel- berg, 2014), pp. 13–51
3. A.M. Smith, S. Nie, Accounts of Chemical Research **43**(2), 190 (2010)
4. A.L. Efros, , M. Rosen, Annual Review of Mater. Sci. **30**(1), 475 (2000)

5. S. Gaponenko, *Introduction to Nanophotonics* (Cambridge University Press, Cam- bridge, 2010)
6. M.F. Pereira, Optical and Quantum Electronics **47**(4), 815 (2015)
7. S. Mirov, V. Fedorov, I. Moskalev, M. Mirov, D. Martyshkin, J. Luminescence **133**, 268 (2013). 16th International Conference on Luminescence ICL'11
8. P. Thakur, A. Kumar, S. Gautam, K. Chae, Thin Solid Films **519**(23), 8401 (2011)
9. J. St¨ohr, *NEXAFS Spectroscopy* (Springer-Verlag, Berlin, 1991)
10. Y. Wang, A. Suna, W. Mahler, R. Kasowski, J. Chem. Phys. **87**(12), 7315 (1987) 11. P.V. Kamat, J. Phys. Chem. C **112**(48), 18737 (2008)
12. A.P. Alivisatos, Science **271**(5251), 933 (1996)
13. J.K. Furdyna, J. Appl. Phys. **64**(4), R29 (1988)
14. H. Ohno, Nat. Mater. **9**(12), 952 (2010)
15. ´Ismail. Polat, S. Aksu, M. Altunba¸s, E. Bacaksz, physica status solidi (a) **209**(1), 160 (2012). DOI 10.1002/pssa.201127248
16. H. Ohno, A. Shen, F. Matsukura, A. Oiwa, A. Endo, S. Katsumoto, Y. Iye, Appl. Phys. Lett. **69**(3), 363 (1996)
17. S.A. Wolf, D.D. Awschalom, R.A. Buhrman, J.M. Daughton, S. von Molnr, M.L. Roukes, A.Y. Chtchelkanova, D.M. Treger, Science **294**(5546), 1488 (2001)
18. M. Johnson, J. Phys. Chem. B **109**(30), 14278 (2005). PMID: 16852795
19. S.K. Mishra, R.K. Srivastava, S. Prakash, R.S. Yadav, A. Panday, J. Alloys Comp. **513**(0), 118 (2012)
20. D. Sreekantha Reddy, B. Kang, S. Yu, K. Gunasekhar, P. Sreedhara Reddy, Appl. Phys. A **91**(4), 627 (2008)
21. E. Mittemeijer, U. Welzel, Zeitschrift fu¨r Kristallographie International journal for struc- tural, physical, and chemical aspects of crystalline materials **223**(9), 552 (2009)
22. R.D. Shannon, Acta Crystallographica Section A **32**(5), 751 (1976)
23. M. Diana, G. Mazzone, J.J. DeMarco, Phys. Rev. **187**, 973 (1969)
24. G. Williamson, W. Hall, Acta Metallurgica **1**(1), 22 (1953)
25. B. Warren, B. Averbach, J. Appl. Phys. **21**, 596 (1950)
26. T. Ung´ar, G. Tichy, J. Gubicza, R.J. Hellmig, Powder Diffraction **20**, 366 (2005)
27. H. Nalwa, *Handbook of nanostructured materials and Nanotechnology*, vol. 2 (Academic Press, 2000)
28. T.H. de Keijser, J.I. Langford, E.J. Mittemeijer, A.B.P. Vogels, J. Appl. Crystal. **15**(3), 308 (1982)
29. R. Young (ed.). *Crystal Imperfection Broadening and Peak Shape in the Rietveld Method*, *The Rietveld Method* (1993)
30. S. Kumar, P. Sharma, V. Sharma, J. Nanopart. Res. **15**(5), 1662 (2013)